X-RAY OPTICS FOR SOFT X-RAY SELF-SEEDING THE LCLS-II

Y. Feng, J. Hastings, P. Heimann, M. Rowen, J. Krzywinski, J. Wu
LCLS, SLAC, Menlo Park, CA 94025, U.S.A.

Abstract

A complete design of the X-ray optics for soft X-ray self-seeding the future LCLS-II is described. It consists of a variable-line-spacing (VLS) grating monochromator for creating a transform-limited seed pulse from a SASE undulator X-ray beam and associated mirrors for imaging the seed pulse into a seeding undulator. The grating is designed to operate in the fixed-focus mode and energy tuning is achieved by rotations of a pre-mirror and the grating. Only one ruling of 2222 lines/mm is needed to cover the entire energy range from 200 to 2000 eV with a nearly constant resolving power of 23000. The grating would produce fully transform-limited pulses of 12 fs (rms) long at 2000 eV or 120 fs (rms) long at 200 eV with sufficient power to seed. The optical system produces a slightly energy-dependent time delay of about 5 ps. The transverse size of the seed beam is nearly identical to that of the SASE beam in the horizontal, but is slightly variable to < 10% of original in the vertical direction depending on the X-ray energy. The resolving power and beam propagation calculations are formulated entirely on the ABCD matrix applied to a full coherent FEL beam.

INTRODUCTION

In many FEL applications, the temporal or spectral properties of the X-ray pulse are of great importance to the quantitative understanding of the experimental measurements especially when non-linear effects are expected. The SASE based FEL's such as the LCLS produce X-ray pulses with extremely high temporal fluctuations that should be eliminated or minimized in future FEL constructions such as the upcoming LCLS-II by certain seeding schemes. One possible approach is that of self-seeding using two undulators, one SASE and one seeded originally proposed by J. Feldhaus et al [1]. The current design follows the same basic principles of the original concept and is described below.

X-RAY OPTICS DESIGN

The complete self-seeding X-ray optics system is shown schematically in Fig. 1. It consists of a cylindrical horizontally focusing mirror $\mathbf{M}_1$, a plane vertically deflecting pre-mirror $\mathbf{M}_2$, a plane vertically dispersing variable-line-spacing (VLS) grating **G**, a vertical exit slit **S**, and a spherical vertically focusing mirror $\mathbf{M}_3$. The trajectory of the e-beam is shown as a reference. The specifications of the grating monochromator are given in Table 1, and only a single grating is used and has a groove density of 2222 lines/mm to cover the entire energy range from 200 to 2000 eV. The monochromator is to operate in the "constant focal-distance" mode [2] as opposed to the "constant included angle" mode and in the +1 order, requiring rotation of both the pre-mirror $\mathbf{M}_2$ and grating **G** for tuning the energy by varying the incidence angle, and diffraction angle while keeping the focus at the exit slit **S**. The nominal object distance r from the source, which is assumed to be one gain length upstream of the downstream end of the 1st SASE undulator, to the centre of the grating is 9 m, and the nominal image distance r' from the grating to the exit slit is 3 m. The first coefficient σ_1 of the VLS grating is ~ -3×10^{-7} as determined by the focusing equation $\sigma_1 = -\sigma^2/\lambda(\cos^2\alpha/r+\cos^2\beta/r')$, where σ, λ, α, β are the grating period, X-ray wavelength, incident and diffraction angles. The focal length has slight energy dependence. Following the plane grating monochromator scheme, the rotation of the $\mathbf{M}_2$ is pivoted at a point directly above the centre of the grating, and during energy tuning the beam walks along the surface of $\mathbf{M}_2$. The direction of the beam is fixed between $\mathbf{M}_1$ and $\mathbf{M}_2$, and between the grating and the exit slit, but varies between $\mathbf{M}_2$ and the grating during tuning. As such, the total optical path is not fixed as would be in the case of a "constant included angle" mode operation. The de-magnified source at the exit slit is focused before entering the seeding undulator by the mirror $\mathbf{M}_3$. The exit monochromatic beam is designed to be collinear to the incident beam. The re-entrant point is located inside the seeding undulator where the electron beam is re-introduced and merged with the seed X-rays.

Resolving Power

The maximum achievable resolving power of the grating is shown in Fig. 2 which approaches 23000 at 2000 eV and is roughly constant over the designed energy

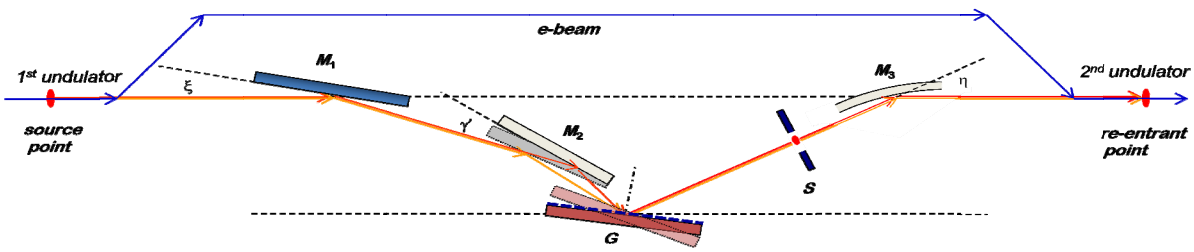

Figure 1: Schematics of the optics for soft X-ray self-seeding the LCLS-II.

range, and is sufficient to produce temporally transform-limited seed pulses with durations of 120 fs (rms) at 200 eV and 12 fs (rms) at 2000 eV. The estimate of the resolving power included contributions from the size of the FEL source inside the SASE undulator, the size of the exit slit in the dispersion plane assuming to vary from 2 μm at 2000 eV to 10 μm at 200 eV, slope error of the grating and optical aberrations. The grating performance was calculated using the ABCD matrix method [3] applied to fully coherent Gaussian beams [4] and for VLS gratings [5]. The high resolving power is achieved due to the high demagnification at the exit slit.

Table 1: Grating Specifications

Parameter	**Symbol**	**Value**	**Unit**
Line spacing	σ	0.45	μm
Order	n	+1	
Linear coeff.	σ_1	-3.0225×10^{-7}	
Groove height	h	5.393	nm
Grating profile		Lamella/Steps	
Incident angle	θ	4.79 – 15.1	mrad
Exit angle	θ'	52.7 – 166.9	mrad
Included angle	2Θ	176.7 – 169.6	degree
Object distance	L_{obj}	~ 9	m
Image distance	L_{img}	~ 3	m
Exit slit size	S	2 – 10	μm

Resolving Efficiency

A simple calculation assuming a lamellar grating profile and complete shadowing of the groove was used to estimate the grating efficiency as shown in the right panel of Fig. 2 (yellow curve) , and a more sophisticated method based on wave propagation gave similar but lower values (purple crosses). The low efficiency was due to the incidence and diffraction angles being greater than the critical angle of the grating coating assumed to be Boron.

Imaging in Dispersion Plane

The incident X-ray beam is imaged at the exit slit and re-imaged at the re-entrant point inside the seeding undulator by a spherical mirror $\mathbf{M}_3$ and the variation of the Gaussian beam waist as a function of tuning energy is shown in Fig. 3, where the image size (purple curve) matches that at the source (blue curve) at 2000 eV, but is smaller by about 10% at 200 eV. The specifications of the mirrors of both vertical collimation and the horizontal focusing mirrors are given in Table 2. The radius of $\mathbf{M}_3$ is 28.881 m, giving a focal length of 137.9 mm at an incidence angle of 9.555 mrad. The exit slit is positioned near the back focal point of $\mathbf{M}_3$ so the very narrow image of the input beam is magnified to a similar size to the original size at the re-entrant point. The distance from $\mathbf{M}_3$ to the re-entrant point is ~ 2 m. The exact location of the waist of the seed beam shifts about the re-entrant point while energy is being tuned due to the coherent nature of the FEL beam propagation, though the maximum shift is ~ 0.16 m or about 1/30 of the Rayleigh length, thus not significantly impacting the seed power density inside the 2nd undulator.

Imaging in Sagittal Plane

In the sagittal plane, the source is imaged in a single step at the exit slit by the cylindrical focusing mirror $\mathbf{M}_1$, and similar dependence of image size on tuning energy is obtained as shown in Fig. 3. The radius of $\mathbf{M}_1$ is 0.133 m, giving a focal length of 4.926 m at an incident angle of 13.5 mrad. Maximum shift in the exact location of the waist is ~ 0.32 m or about 1/15 of the Rayleigh length and thus has negligible effect on the seed power density.

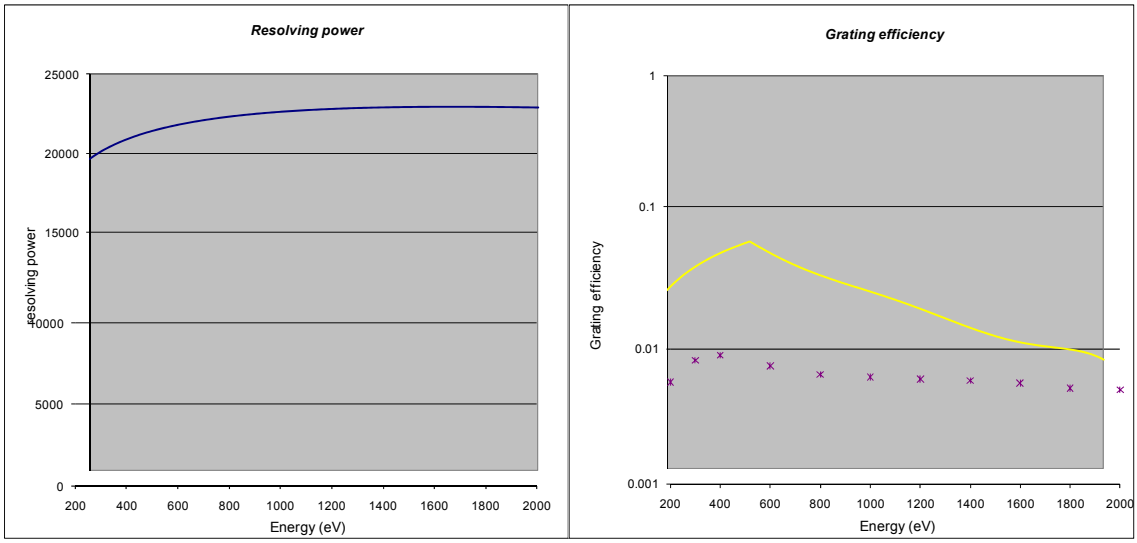

Figure 2: Resolving power and efficiency of the grating monochromator.

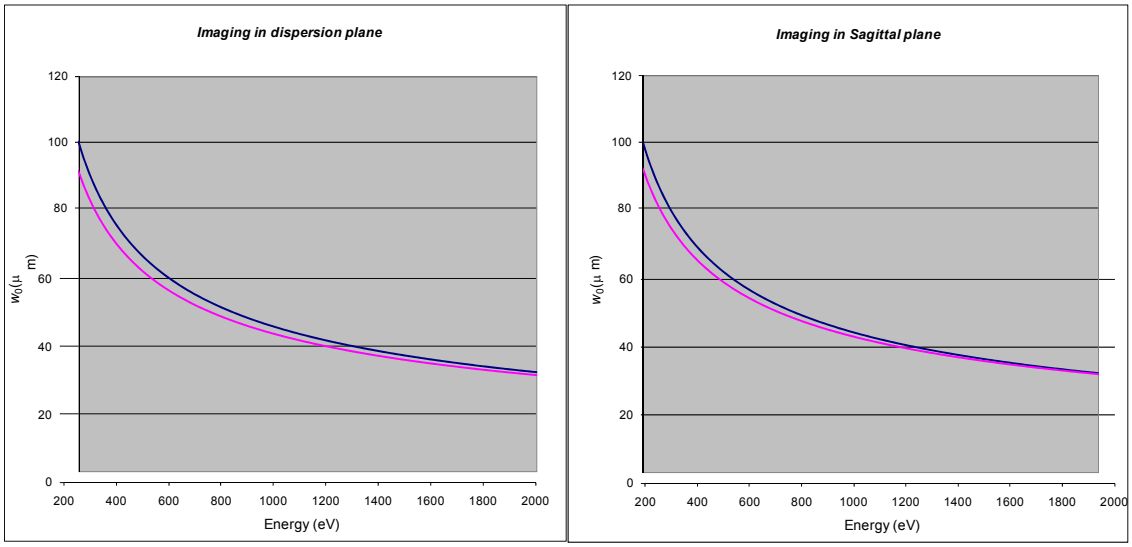

Figure 3: Imaging in vertical (dispersion) and sagittal planes.

Table 2: Specifications of mirrors

Parameter	Symbol	Value	Unit
Cylindrical mirror radius	R_1	0.1330	m
focal length	f_1	4.9261	m
Incident angle	ξ	13.50	mrad
Planar mirror radius	R_2	∞	m
Incident angle	γ'	5.700 – 67.93	mrad
Spherical Mirror radius	R_3	28.8807	m
focal length	f_3	0.13790	m
Incident angle	η	9.555	mrad

Output Seed Power

The output power of the seed beam at the re-entrant point was calculated and shown in Fig. 4 by assuming a certain input power (blue curve in left panel in Fig. 4) and using the bandwidth reduction by the monochromator and the simple efficiency estimate (purple curve) and more rigorous calculation (yellow triangle). The necessary power for effective seeding is shown as the cyan curve which is smaller than the expected output of the seed beam.

Optical Delay

The optical delay is ~ 5 ps and its energy dependence is shown in the right panel of Fig. 4. The delay is not constant but varies with the energy due to the X-rays reflecting off $\mathbf{M}_2$ at different points and taking different optical paths as energy is being tuned. The e-beam excursion time needs to match this variation for maintaining time overlap with the seed pulse.

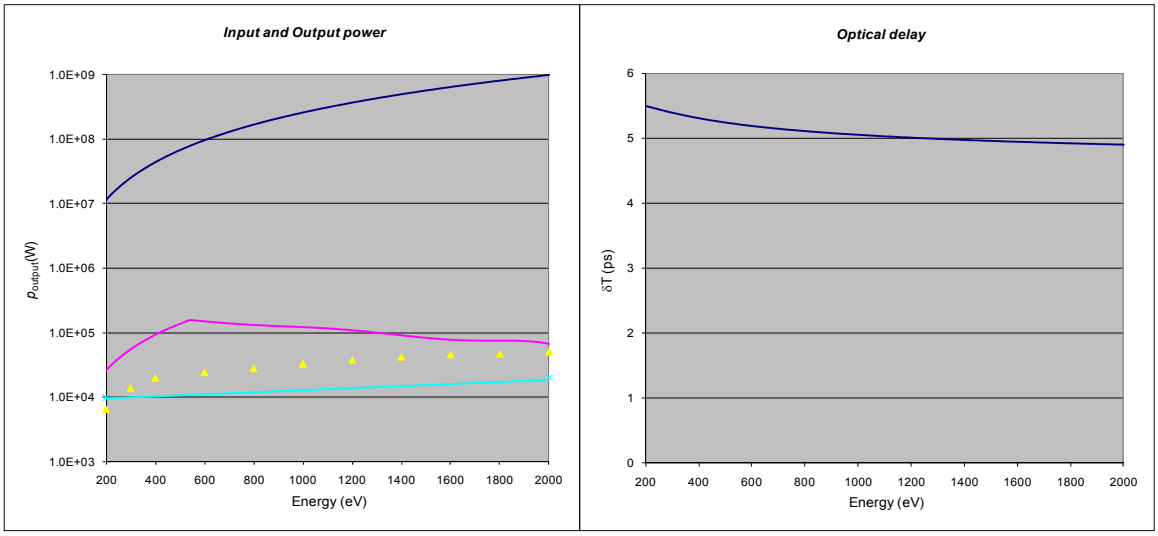

Figure 4: Output seed power and optical delay

Ray-tracing Results

Ray-tracing was performed which verified the designed performance including the resolving power, imaging at the re-entrant point both by the cylindrical focusing and the spherical collimation mirrors. There are aberrations by the $\mathbf{M}_3$ mirror due to the large magnification needed to return the small vertical beam size at the exit slit to its original value at the re-entrant point.

In summary, a complete optical system for self-seeding the future LCLS-II is described, and its performance meets all requirements in resolving power, imaging, and output power.

REFERENCES

[1] J. Feldhaus et al, *Optics Communications*, **140**, p.341 (1997);

[2] H. Peterson, *Optics Communications*, **40**, p.402 (1982);

[3] B. Saleh and M. Teich (1991). *Fundamentals of Photonics*. New York: John Wiley & Sons. Section 1.4, pp. 26 – 36;

[4] *ibid.* Section 1.4, pp. 98 - 100;

[5] A. April and N. McCarthy, *Optics Communications*, **271**, p.327 (2007);